

Revisiting a model-independent dark energy reconstruction method

Ruth Lazkoz, Vincenzo Salzano, and Irene Sendra

*Física Teorikoa eta Zientziaren Historia Saila, Zientzia eta Teknologia Fakultatea,
Euskal Herriko Unibertsitatea, 644 Posta Kutxatila, 48080 Bilbao, Spain*

(Dated: June 11, 2022)

Model independent reconstructions of dark energy have received some attention. The approach that addresses the reconstruction of the dimensionless coordinate distance and its two first derivatives using a polynomial fit in different redshift windows is well developed [4–6]. In this work we offer new insights into the problem by focusing on two types of observational probes: SNeIa and GRBs. Our results allow to highlight some of the intrinsic weaknesses of the method. One of the directions we follow is to consider updated observational samples. Our results indicate that conclusions on the main dark energy features as drawn from this method are intimately related to the features of the samples themselves (which are not quite ideal). This is particularly true of GRBs, which manifest themselves as poor performers in this context. In contrast to original works, we conclude they cannot be used for cosmological purposes, and the state of the art does not allow to regard them on the same quality basis as SNeIa. The next direction we contribute to is the question of how the adjusting of some parameters (window width, overlap, selection criteria) affect the results. We find again there is a considerable sensitivity to these features. Then, we try to establish what is the current redshift range for which one can make solid predictions on dark energy evolution. Finally, we strengthen the former view that this model is modest in the sense it provides only a picture of the global trend. But, on the other hand, we believe it offers an interesting complement to other approaches given that it works on minimal assumptions.

PACS numbers: 95.36.+x, 98.80.-k

Keywords: dark energy

I. INTRODUCTION

It is very timely to continue to explore the acceleration of the Universe [1], as its discovery has very recently finally gathered the top recognition of the community. The question of whether such evolution is produced by a dark energy component or rather a manifestation of bold unknown Physics remains one of the most puzzling topics in Cosmology [2]. Assuming the dark energy scenario, and beyond theoretical questioning about its physical nature, it is most vital to learn to extract the best and most relevant information from current astronomical data. Many methods are strongly tied to the assumption of a background cosmological model or, equivalently, of an analytical dark energy equation of state (EoS). Such is precisely the case of the reconstruction of the Hubble diagram of type Ia Supernovae (SNeIa), which provided the first evidence for the acceleration of the Universe [1]. The diagram presents the corresponding distance modulus at different redshifts and is computed from the EoS itself after a convenient integration in redshift. Variations of this procedure apply as well when considering other observational tests such as gamma ray bursts (GRBs), baryon acoustic oscillations (BAO) or the cosmic microwave background (CMB). But even though biases on final results may depend on the previously described assumptions, that route, and in particular giving a specific prescription of the EoS is still the most popular data analysis method, as opposed to model independent methods (EoS free prescriptions) for the reconstruction of dark energy. Fortunately, literature sources about this alternative way to explore the accelerated universe have

mounted considerably, and thus the state of the art has turned promising [3].

In [4–6] the authors present a different approach to this model independent reconstruction: the dimensionless coordinate distance and its first and second order derivatives with respect to redshift are reconstructed using a polynomial fit inside an appositely designed redshift window. The only underlying assumption is a description of the Universe by a generic Friedmann-Robertson-Walker (FRW) metric. Moreover, the method does not depend on the physical properties of the components of the Universe or on the underlying gravity theory. The latter is an aspect to be considered only at a second stage, when one attempts at the derivation of the behavior of more interesting and observable cosmological quantities: the dimensionless expansion rate $E(z) \equiv H(z)/H_0$, the universe acceleration (through the well known deceleration parameter $q(z) \equiv -\ddot{a}a/\dot{a}^2$), or finally the dark energy EoS parameter $w(z) \equiv p_{de}/\rho_{de}$. As usual, here a is the scale factor, the dots denote derivatives with respect to cosmological time, and p_{de} and ρ_{de} are respectively the dark energy pressure and density.

In this work we aim at a thorough and novel study of a number of main aspects of this problem. Firstly, observational samples are updated, and results with [6] are compared, as far as possible. This lets us verify that, opposite to what one could expect *in principle*, conclusions in general are strongly related to the way observational samples have been built on. This is not, thus, a caveat of the reconstruction method, and could rather be useful at a first observational level so as to discern the requirements a sample needs to be useful for the inference of

information about dark energy. Secondly, the validity of GRBs in the context of this method is checked. It has been pointed out [6] that these data can be a promising tool to study cosmology at high redshifts. In this regard, our results seem to hint that GRBs are not as compelling as desirable, and probably the reasons for this are intrinsic to the nature of actual GRBs observables. This is in agreement with the critical view in [7].

After this, it is argued that the analysis in the model independent spirit of [6] requires adjusting some parameters. But typically, this causes noise and large errors in some regimes (this seems to be intrinsically related to the procedure itself). Thus, the following questions arise quite naturally: how can the real cosmological information be *read off* from these noisy patterns? And how and when can the goodness and closeness to reality of the reconstructed profiles be ascertained?

At the next stage, we move on to explore the range of application of the method and compare it with the results obtained using a specific dark energy EoS. At the same time, we investigate how physically relevant parameters depend on the errors and noise of data.

Finally, we conclude that this method just provides an idea of the global trend of the parameters. The large correlation among them does not allow to obtain independent measures. But, on the other hand, it is admissible to report values associated with independent redshift bins.

In Sec. II we revise the method in its main aspects; in Sec. III we briefly describe the observational tools chosen for the analysis, namely the SNeIa and GRBs samples with their properties; in Sec. IV we discuss the main results both for real and mock data; in Sec. V we present results from the binning approach; and in Sec. VI we summarize the most important results.

II. METHOD

A. Basic quantities

The use of SNeIa and GRBs makes us focus mainly on the distance modulus μ , which is an observable quantity defined as

$$\mu(z) = 5 \log_{10}[D_L(z)] + \mu_0. \quad (1)$$

Here D_L is the luminosity distance (see below), the nuisance parameter μ_0 encodes the absolute magnitude M of any SNeIa and the Hubble constant H_0 (the current value of the expansion rate). For convenience, the speed of light has been set to one, and this choice will apply to the whole paper.

In full rigour, though, a proper model-independent analysis of the GRBs data cannot be based on the GRBs distance modulus, which is not directly observable and depends on the cosmology assumed [8]. As we will discuss in IIIB, we have used a GRBs sample whose cali-

bration is independent of the cosmological model and is based on the use of SNeIa as calibration tools.

The luminosity distance can be written as

$$D_L = H_0^{-1}(1+z)y(z). \quad (2)$$

where the dimensionless coordinate distance $y(z)$ reads explicitly

$$y(z) = \int_0^z \frac{dz'}{E(z')}. \quad (3)$$

The determination of the coordinate distances from the underlying observational data typically proceeds under the assumption of a cosmological model, which reflects in the analytical expression of $E(z)$, the dimensionless expansion rate.

The method developed in [4] does not require any assumption on the cosmological model, or on the expression of the dark energy functional. It is possible though to determine $y(z)$ in a model independent way. Then, as determining the Hubble function $H(z)$, and deceleration parameter $q(z)$ only involves the computation of the derivatives of $y(z)$, those two quantities of interest inherit the model independence.

The method was developed by [4] and follows a series of steps which we describe in the next subsection.

B. Inputs and fits

Step 1. The input data needed are the collection of (z_i, y_i, σ_i^2) , quantities, where the index i ranges from 1 to \mathcal{N} (the number of objects in the chosen dataset). Let us describe those quantities one by one. Clearly, the z_i are the redshifts for the dataset objects. Then, the $y_i = y(z_i)$ denote the coordinate distance data values obtained from the observational quantities (as the observed variable is $\mu(z)$, Eqs. (1) - (2) have to be combined to give the y_i). Finally, the σ_i^2 represent the coordinate distance errors. Contributions to this last quantities will come both from errors on $\mu(z_i)$ and from errors on the redshifts z_i . The sample we have used was not presented with errors on the redshifts, but using old dataset values, we have verified that the redshift contribution from those errors is always negligible when compared to the contribution from the errors in the $\mu(z_i)$.

Step 2. We define a redshift grid with the values z_j , and at each of them we evaluate the coordinate distances, their derivatives and the related cosmological quantities. The properties of this grid are completely arbitrary, but we have checked this does not affect final results; in our case the grid will range from 0 until the maximum redshift z_{max} reached by the chosen dataset, with an homogeneous spacing of 0.005.

Step 3. Finally, we have to perform a weighted polynomial fit of (z_i, y_i) , with the inverse errors $1/\sigma_i^2$ as statistical weights. The fit is not, though, a global one. We rather do a number of individual fits in separate redshift

windows defined by a length Δ_f and a center z_0 . For each fit just those data points falling in each window are taken, and the central redshift moves iteratively along the grid values z_j . At both ends of each window, we apply in addition a Gaussian tapered region with dispersion σ_g and extending out to $2\sigma_g$. This makes all the points in this region have their weights reduced by the value of the Gaussian wing at that point. This way, fluctuations and discontinuities are controlled when moving from one window to another. Then the fit is performed after changing the variables from z_i to $x_i = z_i - z_0$, so that the coordinate distance values and its derivatives at $z_0 = z_j$ are simply the values of the coefficients of the polynomial evaluated in $x = 0$. For example, when using a second order polynomial:

$$y(x) = a_0 + a_1x + a_2x^2, \quad (4)$$

we will have

$$y(0) = a_0, \quad y'(0) = a_1, \quad y''(0) = a_2; \quad (5)$$

where the prime denotes differentiation with respect to x (or, equivalently, to redshift, in this case). All the cosmological quantities depend on combinations of the respective $(y(0), y'(0), y''(0))$, and the errors can be easily evaluated by straightforward application of error propagation theory.

C. Outputs and derived quantities

The method described in the previous subsection produces a set of j polynomial-reconstructed dimensionless coordinate distance values with their first and second order derivatives values (here j is an integer depending on the redshift grid range and spacing). This allows giving the next step in the reconstruction.

Assuming an FRW metric and no contribution from spatial curvature, one can easily obtain estimations for more cosmologically interesting quantities. One of them is the expansion rate, which from Eq. (3) is easily derivable to be

$$E(z) = (y')^{-1}, \quad (6)$$

where the prime indicates differentiation with respect to redshift. Likewise, the deceleration is given by

$$q(z) = -\frac{\ddot{a}a}{\dot{a}^2} = -1 - (1+z)\frac{y''}{y'}. \quad (7)$$

This expression is obviously valid for any cosmological scenario based on an homogeneous and isotropic expansion. If we now also assume a theory of gravity (in this case General Relativity), we can use the Friedmann equations:

$$\frac{\ddot{a}}{a} = -\frac{4\pi G}{3}(\rho_m + \rho_{DE} + 3p_{DE}), \quad (8)$$

$$\left(\frac{\dot{a}}{a}\right) = \frac{8\pi G}{3}(\rho_m + \rho_{DE}), \quad (9)$$

where ρ_m is the mass-energy density of non-relativistic matter, ρ_{DE} is the mass-energy density of the dark energy, and p_{DE} is the pressure of dark energy. It is straightforward to derive from them the expression of the dark energy equation of state w . Using the standard definition of the critical density at the present epoch, $\rho_{0,c} = 3H_0^2/(8\pi G)$, the dark energy pressure can be shown to be

$$\begin{aligned} p_{DE}(z) &= \rho_{0,c} \left[\frac{E^2(z)}{3} (2q(z) - 1) \right] \\ &= \rho_{0,c} \left[-(y')^{-2} \left(1 + \frac{2}{3}(1+z)\frac{y''}{y'} \right) \right]; \end{aligned} \quad (10)$$

while the dark energy density is

$$\rho_{DE}(z) = \rho_{0,c} [(y')^{-2} - \Omega_m(1+z)^3], \quad (11)$$

where $\Omega_m = \rho_m/\rho_{0,c}$ is the fractional contribution of non-relativistic matter to the critical density at zero redshift, and the term $(1+z)^3$ defines its time evolution. Then, as the dark energy EoS parameter $w(z)$ is defined as the ratio of the dark energy pressure to density, $p_{DE}(z)/\rho_{DE}(z)$, it finally results in the expression

$$w(z) = \frac{-[1 + (2/3)(1+z)y''(y')^{-1}]}{1 - \Omega_m(1+z)^3(y')^2}. \quad (12)$$

Note that Ω_m is clearly involved in the determination of the $w(z)$ parameter and of its related error; here we use the value corresponding to the wcdm+sz+lens case from WMAP7-year [9], which has $\Omega_m = 0.259^{+0.099}_{-0.095}$. Nevertheless, this particular choice does not have a strong impact in the conclusions to be reached.

To close this section let us mention that errors on all the previous quantities are of course derived from errors from y , y' and y'' applying the usual error propagation rules.

III. CURRENT DATA

A. Supernovae

Our main reconstruction tool is one of the most recent type Ia supernovae sample available, the Union2 sample described in [10]. This compilation is the result of a new dataset of low-redshift nearby-Hubble-flow SNeIa and is built with new analysis procedures suitable for working with several heterogeneous SNeIa compilations. It includes the Union data set from [11] with six added SNeIa first presented in [10], along with SNeIa from [12], the low- z and the intermediate- z data from [13] and [14] respectively. After the application of various selection cuts to create a homogeneous and high signal-to-noise data set, $\mathcal{N}_{\text{SNeIa}} = 557$ SNeIa events distributed over the redshift interval $0.015 \leq z \leq 1.4$ were obtained.

The use of the Union2 SNeIa data rests on the definition of the distance modulus as given above. Given the heterogeneous origin of this dataset, and the procedures described in [11] for reducing data, it turns out we need to fix the value of μ_0 for converting the modulus distance $\mu(z, \mu_0)$ to the coordinate distance $y(z)$. One way would be using just low redshift SNeIa to find the best fit value for H_0 starting from the approximate expression valid for this range, $D_L \approx z/H_0$; alternatively, one could assume an independent measurement of the same quantity, as in [16].

Nevertheless, we have chosen a different way to proceed: as we will try to compare results from SNeIa with results from GRBs, choosing the same unique value for H_0 makes sense, even though it is not fundamental for the final results. For this reason, as the GRBs calibration has been done assuming a well fixed value of $H_0 = 70$ (km/s)/Mpc [6, 15], we have decided to use the same value of H_0 for the SNeIa (which at the same time we have tested to give a very good fit to the Hubble diagram of SNeIa at low redshifts).

B. Gamma Ray Bursts

Working out and interpreting results from a GRBs analysis is not an easy task, as the errors on their observable quantities are much larger than those for SNeIa, besides the fact their source mechanism is still not well understood. For this reason, choosing a good GRBs sample is crucial; we have chosen to work with the sample described in [17]. There the authors performed a new calibration procedure on the widely used GRBs sample from [15], which matches perfectly some of the requirements in this paper. The possibility of a comparison between SNeIa and GRBs is strictly related to the building of a Hubble diagram for GRBs too, which is an extremely difficult task because GRBs are not standard candles, unlike SNeIa. To create an Hubble diagram for GRBs, one has to look for a correlation between a distance dependent quantity and a directly observable property. Starting from some of the many correlations that have been suggested not long ago, in [15] the authors created a sample of 69 GRBs in the redshift range $0.17 < z < 6.6$ for which the Hubble diagram is well settled.

Then, in [17] that sample was updated in many aspects, the main one being the test of a new method for the calibration of GRBs based on the non assumption of a priori cosmological model. Such a model independent calibration is built on the idea that SNeIa and GRBs at the same redshift should exhibit the same distance modulus. In this way, interpolating the SNeIa Hubble diagram gives the value of $\mu(z)$ for a sub-sample of GRBs which lies in the same redshift range. This sub-sample can be finally used to calibrate the well known GRBs correlations and, assuming that this calibration is redshift independent, it can be extended to high redshift GRBs. With this procedure, in [17] the authors were able to convert

the [15] sample to a new one, with the same number of objects but with SNeIa-calibrated GRBs distance modulus.

IV. RESULTS

We remind that the main objective of this kind of approach is not to obtain independent measurements of coordinate distances and their related quantities, but rather to find out the global trends underlying the data. More exactly, we aim to specify a possible way of proceeding for optimizing the use of this approach. In particular, we will examine the effects produced by changes in the fitting windows which should enable to detect and distinguish *global* and *local* trends.

On the one hand, as it is well known, using larger fitting windows leads to more robust fits, as more points are included in the analysis; but, at the same time, a strong correlation arises among the various values one obtains, as the fitting windows clearly overlap.

On the other hand, using narrower fitting windows, makes it possible to find local (in a redshift sense) properties of the global trend, and with more redshift resolution. The negative counterpart is that smaller windows also imply working with fewer data points, and this accentuates noisy features in the estimated parameters.

If one assumes implicitly the physically reasonable hypothesis that the coordinate distance $y(z)$ is a smooth function of redshift (as one does in this kind of approach), then one can compare large (global) and small (local) fitting windows results. In that way, one can explore the global trend and the characteristics that depend on local irregularities coming from, for example, mixing heterogeneous sub-samples, even if they are treated appropriately, as is the case of the Union2 sample, or containing intrinsic and physically important information about the universe dynamics. By comparing results from large and small fitting windows, one can detect more clearly reconstruction features due to the limitations of the method rather than to an intrinsic relation to the physics dynamics. In this work we study which is the best range to obtain this information, and we also gather some further understanding about the limits of the method presented: we basically conclude the limits depend on the characteristics of the datasets and the specifications of the fitting windows. We have also performed an independent binning sketch, which has consisted in dividing the data points into a number of bins which do not overlap, and obtaining independent estimations of the required parameters afterwards.

A. SNeIa: comparison with literature

To avoid misunderstandings, let it be clear that there are a number of facts that preclude a very close comparison of our results with those in [6]. To begin with,

our SNeIa sample has two main differences with respect to the samples used in [6]. First of all, the sample we consider is made up of 557 objects as opposed to the 192 in Davis' dataset. This mainly implies a higher mean number density for the data points which should translate into a better knowledge of the global tendency of the parameters under study. This newer sample displays a quite larger number density for $z < 1$, but no considerable changes occur for higher redshifts values, so one still has to be careful about conclusions based on the results in this range. Second, the sample we use is made of different heterogeneous SNeIa sub-samples and, even though data reduction has reduced differences considerably, it is possible that those disparities influence the local properties of our derived quantities.

A quite important new point in our analysis is that we have noticed that some remarkable oscillations that arise at some levels of the reconstruction are not directly due to the fitting algorithm, but mainly related to the presence of SNeIa with a high relative error. To back up this view, we produced a cut version of the total Union2 data sample by deleting all the data points whose error was larger than $\langle err \rangle + 2 \sigma_{err}$, where $\langle err \rangle = 0.225$ is the mean of the data error distribution and $\sigma_{err} = 0.133$ is its standard deviation. With this procedure we cut 30 points (all having in common a high relative error) and the oscillatory (noisy) features disappeared.

We performed different runs changing both the length of the fitting windows, Δ_f , and the dispersion σ_g of the Gaussian tapered region needed for calculating the fit weights. We regarded as good results just those obtained when the number of data-points inside any fitting window and out of the Gaussian tapered region (i.e. with unchanged error weight) was ≥ 10 , so to assure a minimal sufficient number of data points as compared to the number of fitting parameters. Our choice is slightly stricter than the one proposed in [4].

Fig. 1(a) shows a reconstruction of y derived from a fit with $\Delta_f = 0.6$ and a dispersion $\sigma_g = 0.02$ of the Gaussian tapered region (i.e. the same values used in [6] and regarded there as the *best* ones). The trend is clearly very smooth and quite similar to the one in [6]; all in all, it can be considered as an admirably good reconstruction. We detect, though, that for redshifts $z > 0.8$ there is a slight difference between the reconstructed dimensionless coordinate distance and the theoretically expected one (derived using some updated cosmological models from [9] with respect to the one used in [6]), with a systematic lower trend at high redshifts. Given the location (redshift range) of the deviation, we believe it can put be down to the low number density of SNeIa points in this region.

The reconstruction of the first order derivative of dimensionless coordinate distance y' is clearly less satisfactory. We plot it in Fig. 1(b) using the same redshift range as for the corresponding figure in [6]. Both studies display in a broad sense similar irregularities for $z > 0.6$, but a rise at high redshifts occurs in our case; it is either a hint of a possible systematics in the way high redshift

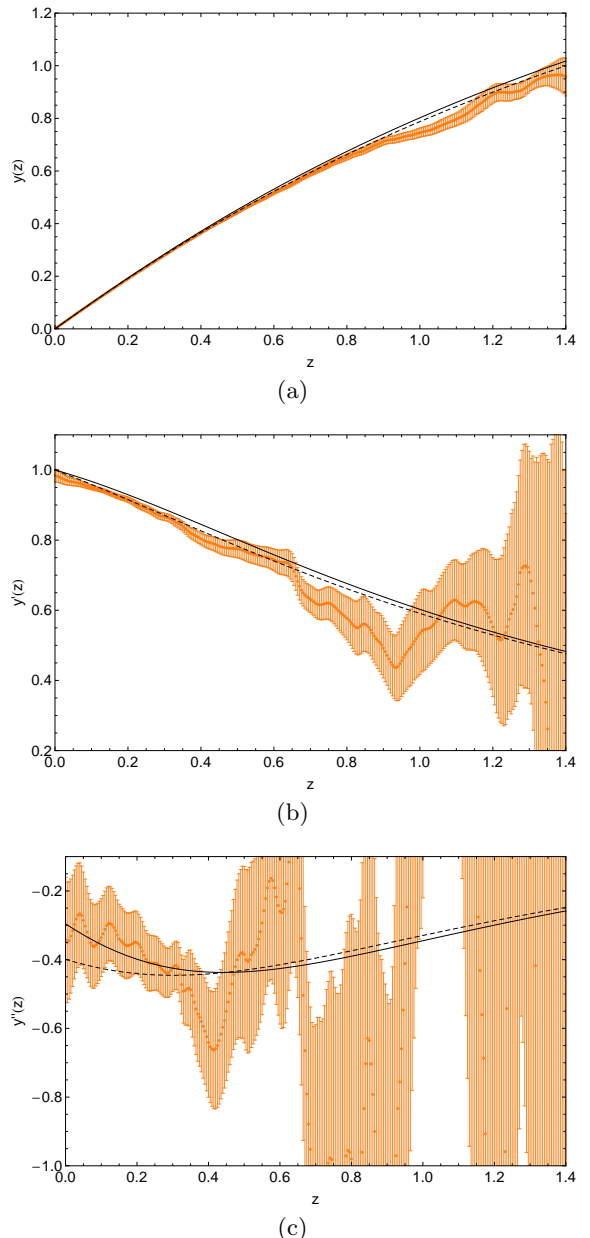


Figure 1. Comparison of $y(z)$, $y'(z)$ and $y''(z)$ with $\Delta_f = 0.6$ and $\sigma_g = 0.02$ from a polynomial analysis with a WMAP7 Λ CDM ($\Omega_m = 0.266$, solid line) and with a WMAP7 (+ WMAP7.2) quiescence model ($\Omega_m = 0.27$, $w = -1.1$, dashed line).

data have been obtained, or it is rather a natural consequence of the low number of data points per bin used in the interpolation, or just a mixture of those such problems. No way of disentangle the two effects is possible at this level.

If we compare this trend in y' with the results about y , it follows immediately that the redshift range where y' rises is the same where y deviates more from the theoretical expectations. We underline that the theoreti-

cal expectations (plotted in the same figures) are only considered as a possible comparison term and a tool for detecting possible local or global properties of the underlying trend. Their use does not mean they are considered important as a fiducial cosmological model.

For what concerns the second order derivative, y'' , Fig. 1(c), we clearly observe a very noisy behavior at redshift $z > 0.4$. This quantity seems more sensitive to oscillations in the number density in SNeIa sample. We reach this conclusion because while [6] this trend looks quite homogeneous, in our reconstruction it is more accentuated so we are tempted to put it down to the heterogeneous nature of the Union2 sample. Thus, even though we are working with a larger SNeIa sample, error bars are quite comparable and, in our case, even larger at high redshift. So, the first lesson one can derive is that denser and larger (in a number data point sense) samples might not improve the use of the model independent reconstruction method we are analyzing. This can be seen as a limitation of the method itself, and in IV D we look deeper into this problem.

B. SNeIa: general overview

Continuing with our analysis, we have also considered differences arising from the use of different window width values. After several preliminary tests, we have eventually considered as representative results from $\Delta_f = 0.6$ (which is the width used in [6]), and from another two widths: $\Delta_f = 0.4$ and $\Delta_f = 1.0$.

1. How small a window?

As we are working with a data set that contains a statistically significant number of objects, one may be tempted to try and improve the analysis by using smaller redshift windows for the fit, as, *in principle*, one would still have a sufficient number of points. This is, however, not true mainly due to the non uniformity of redshift distribution of our SNeIa sample. We have a large number of objects at small redshifts but too few points are at high redshifts, and this makes the noisy trends and the errors grow in this range. It is thus not surprising that more stringent constraints on our derived quantities at large redshifts cannot be obtained.

Moreover, when the fitting window width becomes smaller, the *extremal* intervals (i.e. intervals at very low and high redshift) become precisely the most problematic cases. We can see this in Fig. 2(e) by paying attention to the case of the reconstructed y'' . Note that the errors get minimal in the mid redshift range, but then grow again for low (large number of data points) and high (small number of data points) redshifts. On broad terms, at low redshifts the number of datapoints in typical windows is high, and so we have small noisy oscillations and biased estimations of the reconstructed parameters, but

estimations also depend on the Gaussian tapered region dispersion, σ_s . In contrast at high redshifts, few points will be found in our window, and constraints are poor: many oscillations and large error bars occur.

2. How large a window?

On the other hand, taking into account that our main goal is to guess the global trend of our parameters, we considered a somehow completely opposite approach. Specifically, we studied the effect of enlarging the fitting window as much as possible so as to detect a global and unified trend of the data (even though this would cause overlaps in the fitting windows and a related growth in the correlation). We detected that large fitting windows give very smooth trends, mainly because the data are, in some measure *averaged*. But at the same time these results are strongly biased (as already reported by [6]), because the polynomial fit describes very poorly the general trend of our quantities. More specifically, a second or third order polynomial can fit *very well* the dimensionless coordinate distance in the redshift range depicted by data, but it would give strongly unphysical trends when extended to higher (out of sample) redshifts as, for example, a negative coordinate distance. For this reason, we do not present here cases with widths wider than $\Delta_f = 1.0$, because this is the largest amplitude for which such a bias has a negligible effect on our reconstructed quantities.

3. Parameter estimates

Let us review now our estimations of several parameters, obtained under the considerations described above.

a. Hubble parameter The reconstructed Hubble diagram hardly changes for the three different windows lengths considered. As we show in the zoomed vision of Fig. 2(b), differences are negligible and no significant discrimination is possible when compared with Union2. We have to recall the good behaviour of the reconstruction of this quantity. The reconstructed Hubble parameter, Fig. 2(d), is practically independent of the fitting window for $z < 0.5$, and in this redshift range it fits quite well the observational data extracted from differential ages of passively evolving galaxies and discussed in [18]. The Hubble constant (i.e. $H_0 = H(z = 0)$) is found to be:

$$H_0 = \begin{cases} 70.63 \pm 1.85 & \text{for } \Delta_f = 0.4, \\ 71.14 \pm 1.34 & \text{for } \Delta_f = 0.6, \\ 71.04 \pm 1.02 & \text{for } \Delta_f = 1.0. \end{cases} \quad (13)$$

in units of (km/s)/Mpc. Clearly, differences among the three fitting windows are very small, just notice that the larger the window, the lower the error on H_0 . We can also see that the three trends are quite similar up to $z \approx 0.5$,

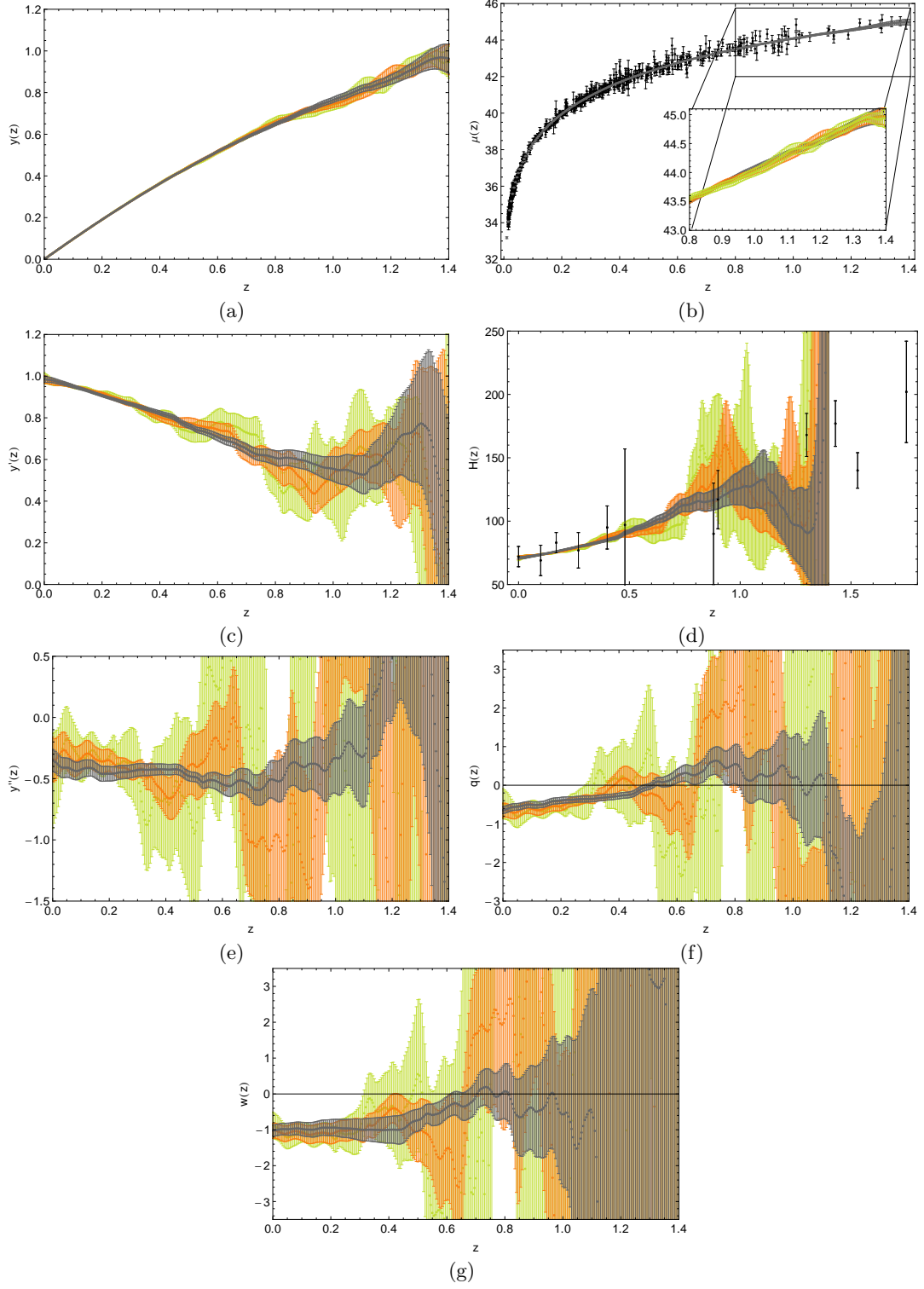


Figure 2. Second order polynomial reconstruction with SNeIa (Union2). Coordinate distance $y(z)$ and its derivatives ($y'(z)$ and $y''(z)$), and the derived cosmological quantities: distance modulus $\mu(z)$, Hubble function $H(z)$, deceleration parameter $q(z)$ and the dark energy EoS $w(z)$. Different colors are used for different fitting window Δ_f : from lightest to darkest for $\Delta_f = 0.4$, $\Delta_f = 0.6$ and $\Delta_f = 1.0$ respectively.

while significant deviations appear for to high redshift data.

b. Deceleration parameter The deceleration parameter $q(z)$, Fig. 2(f) is influenced by the noisy features in $y''(z)$, which become rather important at high redshifts. Differences among the three fitting windows considered become manifest when one calculates the present value of $q(z)$ and z_t (transition redshift from deceleration to acceleration)¹. Our estimates are:

$$q_0 = \begin{cases} -0.477 \pm 0.391, & z_t \sim 0.31 \text{ for } \Delta_f = 0.4, \\ -0.652 \pm 0.185, & z_t \sim 0.38 \text{ for } \Delta_f = 0.6, \\ -0.645 \pm 0.091, & z_t \sim 0.51 \text{ for } \Delta_f = 1.0. \end{cases} \quad (14)$$

Just for comparison, the WMAP Λ CDM model plotted in Fig. 3 has $q_0 = -0.601$ and $z_t = 0.77$, while the WMAP quiescence model $q_0 = -0.704$ and $z_t = 0.74$. In this sense, the reconstruction at low redshifts seems to be consistent with such cosmological models, so we have another proof of the consistency of the method in that regime.

c. EoS parameter It is not an easy task to argue whether the EoS parameter $w(z)$ has a constant or a dynamical behaviour (as it is possible to verify by having a look at Fig. 4): for high redshifts the noise and the errors make it impossible to draw any strong conclusion. Nevertheless, we can offer estimates for the present values:

$$w_0 = \begin{cases} -0.874 \pm 0.369 & \text{for } \Delta_f = 0.4, \\ -1.025 \pm 0.211 & \text{for } \Delta_f = 0.6, \\ -1.019 \pm 0.154 & \text{for } \Delta_f = 1.0. \end{cases}$$

Note that those are all compatible with both the WMAP Λ CDM and quiescence model. Another interesting value is $w_{0.5} = w(z = 0.5)$: following [19] it is worth considering an alternative parametrization for the dark energy EoS, as opposed to the most used [20] Chevalier-Polarski-Linder (CPL) model² [21, 22]. This scenario (specifically, a reparametrization of the former) addresses the values w_0 and $w_{0.5}$, instead of the asymptotic value $w_a = w(z \rightarrow \infty)$ (see footnote). This pair of values has the advantage of lower correlation and informs us about a redshift range well accessible from current data. The reconstructed estimations for this alternative second dark energy parameter are:

$$w_{0.5} = \begin{cases} 0.551 \pm 2.079 & \text{for } \Delta_f = 0.4, \\ -1.058 \pm 0.835 & \text{for } \Delta_f = 0.6, \\ -0.733 \pm 0.307 & \text{for } \Delta_f = 1.0. \end{cases} \quad (15)$$

This result shows more efficiently than the previous ones how difficult it is to extract information from small

fitting windows. Moreover, the largest fitting window width we have chosen is again quite free of biasing effects, and it gives values that are in agreement with those for the smallest window. The values corresponding to $\Delta_f = 0.6$ seem to be consistent with a constant EoS, even though the errors on $w_{0.5}$ are really large. On the other hand, results from $\Delta_f = 1.0$ are more compliant with a varying EoS. Both are also consistent with the results in [23], where the SNeIa Union2 sample was fitted with the $(w_0, w_{0.5})$ model. This is also a possible confirmation that the reconstruction works fine, at least up to $z \approx 0.4 - 0.5$.

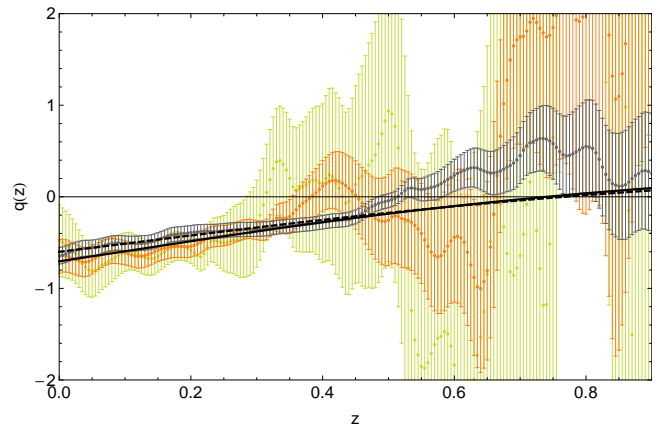


Figure 3. Second order polynomial reconstruction with SNeIa (Union2): reconstruction of the deceleration parameter $q(z)$. Different colors are used for different fitting window Δ_f : from lightest to darkest for $\Delta_f = 0.4$, $\Delta_f = 0.6$ and $\Delta_f = 1.0$ respectively. The solid and the dashed black lines are respectively the WMAP7 Λ CDM ($\Omega_m = 0.266$) and the WMAP7 (+ WMAP7.2) quiescence model.

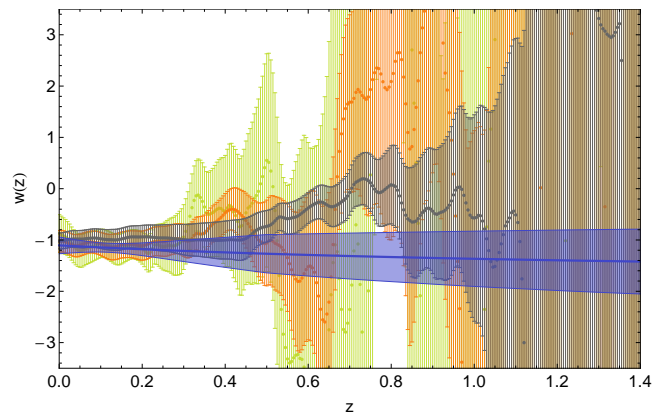


Figure 4. Second order polynomial reconstruction with SNeIa (Union2): reconstruction of the dark energy EoS $w(z)$. Different colors are used for different fitting window Δ_f : from lightest to darkest for $\Delta_f = 0.4$, $\Delta_f = 0.6$ and $\Delta_f = 1.0$ respectively. Blue contours correspond to the best fits for CPL from real data in [28].

¹ Given the noisy behavior it would be more correct to speak about a *first-time* transition redshift, as it is possible that such line is crossed many times more because of the large uncertainties than a real physical source

² As it is well known, the CPL parametrization corresponds to $w(z) = w_0 + w_a(1 - a)$.

C. GRBs

As discussed in the previous related section, the GRBs sample to be used is similar to the one studied in [6], the difference being it is calibrated so that the GRBs Hubble diagram coincides with the SNeIa one in the redshift range where they overlap.

We have performed a cut similar to the one we did for the SNeIa sample: the original data set was approximately homogeneous until a $z \approx 5$ and shows only 2 GRBs for higher redshift up to $z \approx 6.6$. Trying to fit these data is pointless, and all one gets are large noisy trends at their related redshift; for this reason we perform fits without considering these last two points.

The minimum length that can be used with GRBs for which the number of datapoints is higher than the number of parameters is $\Delta_f = 1.3$. Nevertheless, this is a border line case, because the number of datapoints is far too low and in many cases exactly equal to the number of fitting parameters, so that eventual results are statistically invalid. This also gets clearly reflected in the error bars, which are rather big and give no information at all about the trends of the quantities. The minimal number requirement we have also mentioned before (having ≥ 10 points in each fitting window) is first fulfilled by $\Delta_f = 3.0$. For further insight, we also present data from a wider fitting window with $\Delta_f = 4.0$, while one must always keep in mind all the problems that enlarging Δ_f way too much brings about.

In Fig. 5 we can see the reconstructed variables $y(z)$, $y'(z)$, $y''(z)$ for the GRBs sample. The reconstructed $y(z)$ seems to be conditioned by the low number of data points in the sample, which translates into oscillations and growing error bars at high redshifts, larger than those for the SNeIa reconstruction. The first order derivative $y'(z)$ presents two main differences with respect to the SNeIa case: 1. it decreases faster, and most importantly, 2. its present value is sensibly lower. This will have a strong impact in the reconstruction of $H(z)$, which has a strong dependence on $y'(z)$ and becomes manifest in Fig. 5(d). This quantity displays a large deviation from current data, and it results in a very large Hubble constant value (with a large uncertainty as well):

$$H_0 = \begin{cases} 115 \pm 63 & \text{for } \Delta_f = 3.0, \\ 126 \pm 51 & \text{for } \Delta_f = 4.0. \end{cases} \quad (16)$$

These values clearly differ from current accurate estimates from other astronomical probes [16], and no good agreement is found with [18] as the global trend is concerned.

When considering the second order derivative $y''(z)$, represented in Fig. 5(e), one can notice the abrupt change at $z \approx 0.8$, which is also reflected in the related parameters, i.e. $q(z)$ and $w(z)$, as shown in Figs. 5(f) and 5(g). The deceleration and the EoS parameter trends are conditioned by very large error bars; the w profile, in particular, seems to be compatible with a constant EoS,

$w \sim -1$ for $z \leq 0.8$ and $w \sim 0.1$ for $0.8 \leq z \leq 2$; but also becomes divergent at $z \approx 3.5$ due to the denominator entering its expression.

The observed large discrepancy between the GRBs and the SNeIa reconstruction is probably both due to the low number of GRBs data in this regime and to intrinsic shortcoming in the calibration laws required for the treatment of GRBs datapoints. These disadvantage make us feel the GRBs are not reliable to be used in this model-independent framework. However, we expect that an improvement on the knowledge of GRBs can probably lead to tighter measures and then to a better implementation in this method.

D. Mock

The main question arising from the previous section is: what is the degree of confidence on the reconstruction of cosmological quantities with this method? Put in other words, is there any way to discriminate and disentangle the “real” reconstruction from noisy features caused by shortcomings in the algorithm? And considering the particular kind of data we have used, this can also be translated into another question: until what redshift is the reconstruction well based?

To try to throw some light into these matters, we have used a mock SNeIa sample: this is built on a fiducial cosmological model, so that, in theory, if the method works well, one should expect to obtain reconstructed quantities compatible with this model. To create SNeIa mock samples we have taken into account the specifications of the Wide-Field Infrared Survey Telescope (WFIRST) [24], a space mission planned by NASA, which has among its primary objectives to explore the nature of dark energy employing three distinct techniques: measurements of baryon acoustic oscillations, SNeIa distances, and weak gravitational lensing. The redshift distribution of the expected SNeIa to be observed within various redshift bins in a survey of that sort is reported in [25]. The main redshift range extends up to $z \sim 1.6$, with 4 expected SNeIa at $z > 1.6$. The very low redshift subsample, i.e. the 500 SNeIa at $z < 0.1$, is supposed to come from the Nearby Supernova Factory (SNfactory) [26] with measurements in the redshift range (0.03, 0.08), so we are going to assume the former as the lowest redshift value in our mock sample.

Our formulae for errors on SNeIa magnitudes stems from a recipe used in the binning approach [27], which we have however adapted for its application to non-binned data. According to this prescription errors are calculated as follows :

$$\sigma_m^{eff} = \sqrt{\sigma_{int}^2 + \sigma_{pec}^2 + \sigma_{sys}^2}, \quad (17)$$

where: $\sigma_{int} = 0.15$ is the intrinsic dispersion in magnitude per SNeIa, assumed to be constant and independent of redshift for all well-designed surveys; $\sigma_{pec} =$

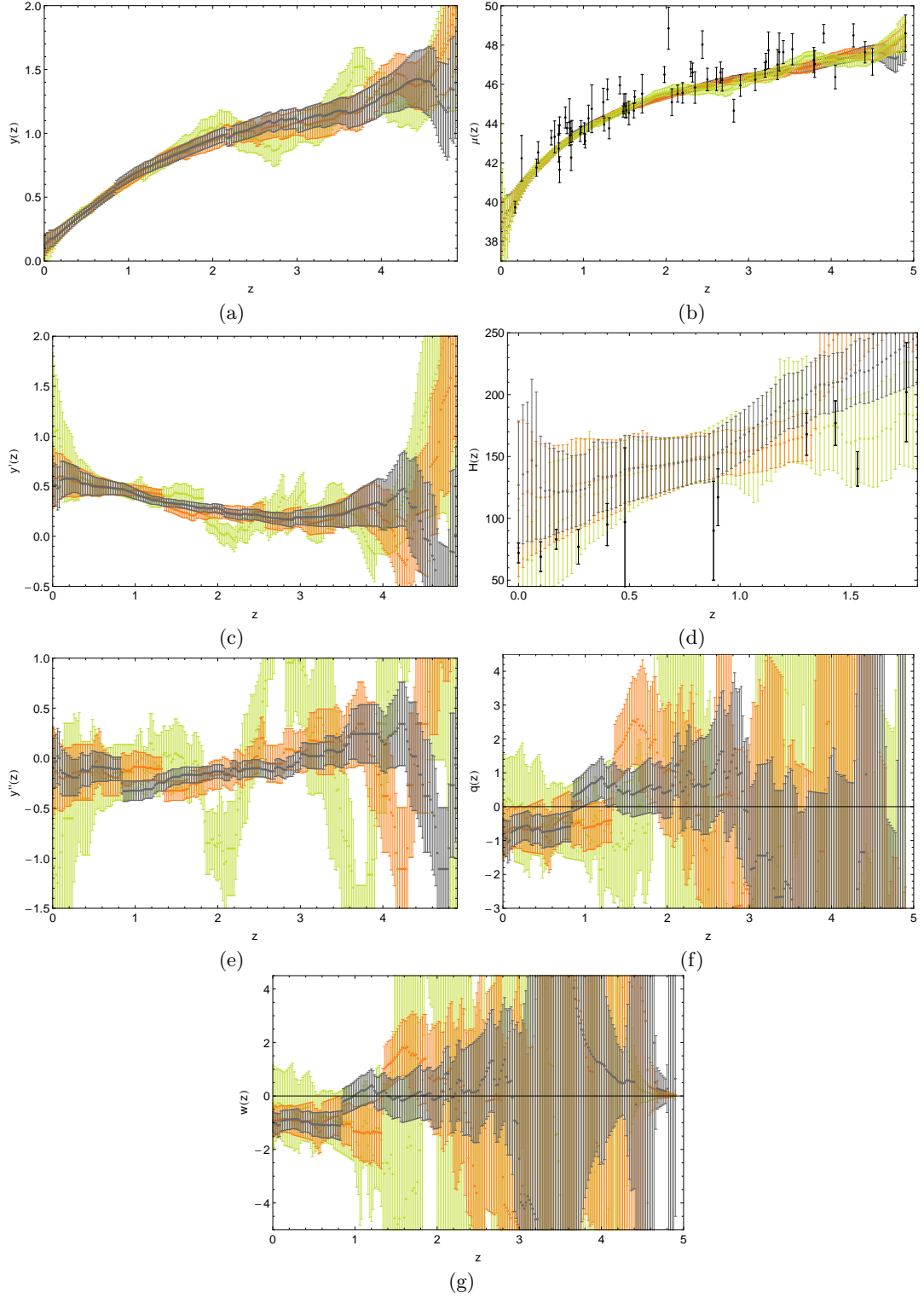


Figure 5. Second order polynomial reconstruction with GRBs (Schaefer-Cardone). Coordinate distance $y(z)$ and its derivatives ($y'(z)$ and $y''(z)$), and the derived cosmological quantities: distance modulus $\mu(z)$, Hubble function $H(z)$, deceleration parameter $q(z)$ and the dark energy EoS $w(z)$. Different colors are used for different fitting window Δ_f : from lightest to darkest for $\Delta_f = 3, \Delta_f = 4$ respectively.

$5\sigma_v/\ln(10)cz$ is the error due to the uncertainty in the SNeIa peculiar velocity, with $\sigma_v = 500$ km/s, c the light velocity and z the redshift for any SNeIa; $\sigma_{syst} = 0.02(1+z)/(1+z_{max})$ is the floor uncertainty related to all the irreducible systematic errors with cannot be reduced statistically by increasing the number of observations. The value 0.02 comes from the fact that WFIRST is a space-based mission (it would be 0.05 for terrestrial-based observations); z_{max} is the maximum observable redshift in the considered mission and this linear term in redshift is used to account for the dependence with redshift of many of the possible systematic error sources (for example the Malmquist bias or gravitational lensing effects). The fiducial model we have used is the Λ CDM+ Ω_m case from WMAP7-year [9], which has $h = 0.75^{+0.15}_{-0.14}$, $\Omega_m = 0.259^{+0.099}_{-0.095}$, and is phantom-like with $w = -1.12^{+0.42}_{-0.43}$.

We will use a mock sample generated with that prescription to study the relation of the proposed reconstruction method with three different features: 1. data dispersion; 2. changes in the fitting window length and 3. the range of validity of the method.

The first point is addressed starting from the algorithm used to generate the mock sample. We take a set of values of the cosmological parameters in the fiducial model which comprises these cases: the best fit, the best fit plus the 1σ error, and the best fit minus the 1σ error. We then construct all possible combinations of them, and then for these sets, and for any redshift in the sample, we find the largest possible variation in the distance modulus. We store this set of values as they are going to serve as our dispersion seeds. The next step is to build four mock samples as follows. We take the distance modulus corresponding to each redshift according to the fiducial model, and then we add to it a random value extracted from a Gaussian centered at zero and with a dispersion which is a number of times (0, 0.25, 0.5 or 0.75) the corresponding value from our dispersion seeds vector. The first case corresponds to mock data points that perfectly resemble the exact fiducial model, while the last value gives a more realistic dispersion similar to the from the present Union2 sample.

For the sake of clarity, we will show results for a window length $\Delta_f = 0.6$, which is the best case for the Union2 sample. In fact, it should also fare well with WFIRST (recall that with a sample with more points and more dense, the fitting window could be diminished with equally good final results). Moreover, we will restrict the discussion to the deceleration and EoS parameter, which are the two most sensitive parameters to eventual features.

From Figs. 6 it is clear that the reconstruction method depends on the dispersion of the observed data. In fact, an effect of this sort should not come as a surprise, as there is always an intrinsic floor for this dispersion (depending on the physics of the observed phenomena and on the reduction procedure of observational data). Consider, for instance the ideal case of null dispersion, as de-

picted in Figs. 6(a) and 6(b), which means that the only element that makes the data differentiating from the fiducial model is the error on the distance modulus. For this case the reconstruction fails at low and high redshift. As discussed in previous section, at low redshift we have biased estimations of the parameters due to the asymmetry of the fitting window, while at high redshift we have few points in each fitting window. As long as the dispersion grows, the deviation from the fiducial model grows too along with the noisy features, finally reaching the more realistic case (0.75). This one is shown in Figs. 6(g) and 6(h), where results are quite similar to those derived from Union2. It follows that an improvement on the observational measures will be translated into a better reconstruction of the parameters under study. However, it has to be taken into account the limitation at high redshift where the density of points is lower. In Fig. 7 we can also verify how the fitting window influences results: in the ideal case of no dispersion in the data (Fig. 7(a)), effectively the smaller the fitting window, the better the reconstruction, with only small deviation at the high redshift tail, where the density of points drops. In the more realistic case in Fig. 7(b), where a larger dispersion in the data is present, we can see how the choice of the fitting window length is crucial. A large window gives a small bias in the estimation of the parameters; on the other side, smaller windows give a better result, but the noise makes it difficult to understand what is the best choice and up to what redshift we have the best reconstruction.

V. BINNED APPROACH

For completeness, we have also carried out an independent analysis using a binned approach so as to get independent values of the magnitudes of interest at certain values of the redshifts. This is, of course, opposed to the work spirit of the previous sections, which were devoted to the study of general trends of the $H(z)$ or the dark energy properties $q(z)$ or $w(z)$. The procedure we present and discuss in this section can be used as an independent check for theoretical models. We must stress, however, that for this part of our analysis we have considered SNeIa only, given that according to our findings on GRBs they do not stand at the moment on the same quality grounds, at least in what concerns the reconstruction methods considered in this paper.

Our starting point has been to divide the SNeIa data sample into different numbers of redshift bins. Then, using the data points within each of them, we have obtained $y(z)$, $y'(z)$ and $y''(z)$. For this task we have followed basically the steps described in the previous section, but with the slight modification of giving a low probability to the points near the boundaries of the bin.

Results obtained with this approach are presented in Figs. 8 - 10 and in Table V. For $H(z)$ the binned approach is well behaved, and the results agree with those presented in [6]. However, for the dark energy EoS pa-

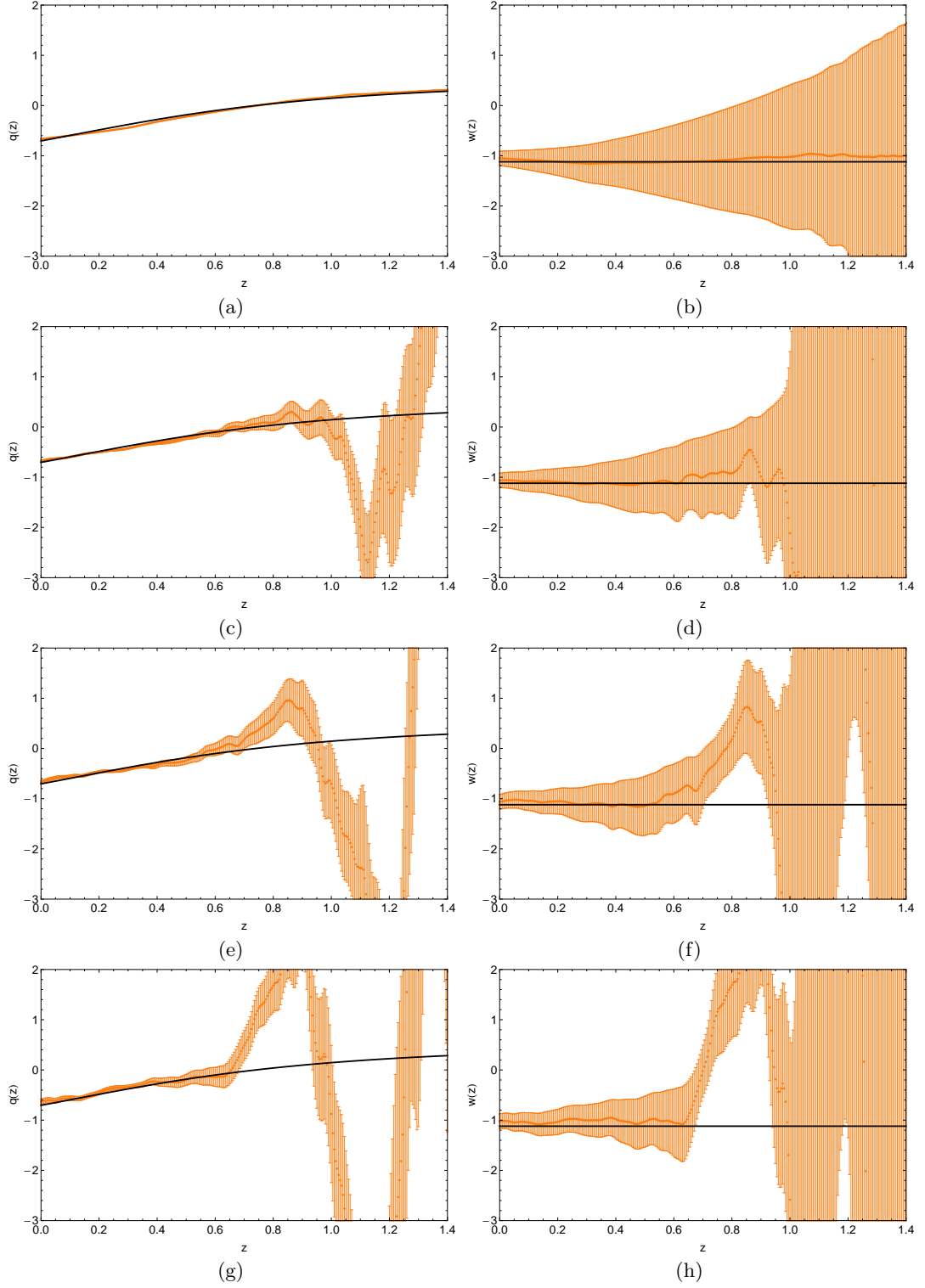


Figure 6. Deceleration $q(z)$ and dark energy EoS $w(z)$ - second order polynomial with WFIRST mock data with $\Delta_f = 0.6$ and $\sigma_g = 0.02$. Black lines are the considered quantities in the fiducial cosmological model used to create the mock data set, the $w_{\text{cdm}} + \text{sz} + \text{lens}$ case from WMAP7-year [9], with $h = 0.75^{+0.15}_{-0.14}$, $\Omega_m = 0.259^{+0.099}_{-0.095}$ and is phantom-like with $w = -1.12^{+0.42}_{-0.43}$. *First panel:* Null dispersion mock data. *Second panel:* Mock data dispersion factor 0.25. *Third panel:* Mock data dispersion factor 0.5. *Fourth panel:* Mock data dispersion factor 0.75. Dispersion values are as described in the related section.

	N	z_{med}	$H(z_{med})$	$w(z_{med})$	$q(z_{med})$
7 bins	77	0.020	72.376 ± 4.717	-21.507 ± 59.869	-23.477 ± 66.523
	76	0.037	89.058 ± 6.928	-17.654 ± 13.774	-21.253 ± 16.817
	77	0.120	74.221 ± 2.238	-0.528 ± 2.985	-0.036 ± 3.027
	77	0.262	84.428 ± 6.905	-10.709 ± 13.375	-9.818 ± 12.307
	76	0.383	72.376 ± 4.717	-21.507 ± 59.869	-23.477 ± 66.523
	77	0.554	89.058 ± 6.928	-17.654 ± 13.774	-21.253 ± 16.817
	76	0.872	74.221 ± 2.238	-0.528 ± 2.985	-0.036 ± 3.027
6 bins	90	0.020	71.263 ± 3.810	-19.860 ± 36.642	-21.380 ± 40.009
	89	0.043	77.258 ± 2.966	-4.103 ± 3.021	-4.170 ± 3.312
	88	0.180	74.085 ± 3.027	-0.502 ± 4.471	0.033 ± 4.160
	88	0.327	77.263 ± 6.982	-3.547 ± 15.760	-2.177 ± 11.795
	89	0.493	82.143 ± 8.881	-3.861 ± 18.912	-1.664 ± 10.408
	90	0.817	108.020 ± 11.380	-0.372 ± 5.025	0.306 ± 2.510
5 bins	108	0.021	70.236 ± 2.907	-13.304 ± 23.791	-13.990 ± 25.630
	107	0.054	70.792 ± 1.973	-0.528 ± 1.393	-0.057 ± 1.467
	107	0.254	81.099 ± 3.568	-0.449 ± 5.014	0.083 ± 4.657
	106	0.438	93.850 ± 9.979	-3.413 ± 10.414	-2.427 ± 8.840
	107	0.769	117.410 ± 12.170	-1.407 ± 3.107	-0.535 ± 2.266
4 bins	134	0.023	69.465 ± 2.183	5.196 ± 8.835	6.103 ± 9.345
	132	0.098	71.411 ± 1.535	-0.549 ± 0.976	-0.052 ± 0.979
	132	0.357	82.531 ± 4.939	2.630 ± 5.835	2.607 ± 4.287
	132	0.703	109.330 ± 8.647	-1.077 ± 2.158	-0.269 ± 1.541
3 bins	177	0.024	72.199 ± 1.588	-1.432 ± 1.553	-1.086 ± 1.706
	176	0.216	75.981 ± 1.886	-0.980 ± 1.407	-0.389 ± 1.274
	176	0.598	97.006 ± 5.010	-0.785 ± 1.288	-0.030 ± 0.849
2 bins	264	0.026	71.913 ± 1.105	-1.074 ± 0.395	-0.684 ± 0.418
	264	0.438	89.085 ± 2.712	-0.895 ± 0.496	-0.204 ± 0.389

Table I. Binned values for $H(z)$, $w(z)$ and $q(z)$, where N and z_{med} are respectively the number of data in each bin and the median redshift in each bin.

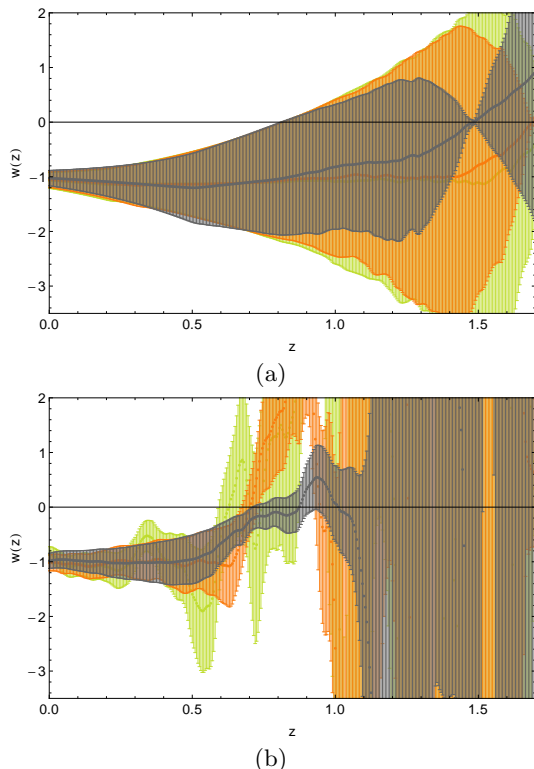


Figure 7. Dark energy EoS function $w(z)$ - second order polynomial with WFIRST mock data. *Left*: mock data with null dispersion and different windows functions (from lightest to darkest, $\Delta_f = 0.4$, $\Delta_f = 0.6$ and $\Delta_f = 1.0$). *Right*: mock data with dispersion 0.75 and different windows functions (from lightest to darkest, $\Delta_f = 0.4$, $\Delta_f = 0.6$ and $\Delta_f = 1.0$).

parameter $w(z)$ and acceleration parameter $q(z)$, we obtain large uncertainties when the number of bins is large. Nevertheless, these uncertainties get smaller as we decrease the number of independent bins and thus increase the amount data within a redshift bin.

VI. SUMMARY AND CONCLUSIONS

The abundant literature sources on model independent reconstructions of dark energy makes one believe this has become a worthy line of investigation. The approach we have been concerned with in this paper has been amply covered in [4–6]. The main idea is to take the dimensionless coordinate distance and try to reconstruct it with minimal assumptions, and then push the reconstruction two levels deeper and consider as well the first and second derivatives with respect to redshift. The way to do this is to carry out polynomial fits in different redshift windows (with carefully chosen characteristics).

We have described the method following the original prescriptions, including throughout additional remarks to facilitate comprehension of the various steps involved. Our main work tool has also been SNeIa luminosity mea-

surements, but we have been benefited by the availability of a sample which offers more than twice the number of sources: the very recent Union2 sample. This clearly allows for some improvement, as increased density of the datasets induces in general tighter constraints. Nevertheless, it must be stressed that the sample considered in our paper is rather heterogeneous.

A fact that seems to have been overlooked in previous references is that the quite noticeable oscillations arising at some levels of the reconstruction are mainly a consequence of data with large error bars in the samples. The fitting algorithm does not seem to be the culprit for these effects. We have been able to reach these conclusions by considering conveniently cut versions of the Union2 sample. The cut produces a spectacular reduction of the noisy features. This suggests it could be worth revisiting this technique when significant advances occur in the compiled datasets. For completeness and comparison we have also performed a similar analysis with GRBs, but the reconstruction turn out to be rather poor (as otherwise expected).

On general grounds we can say the reconstruction from SNeIa is very satisfactory for the dimensionless coordinate, but it degrades considerably as subsequent derivatives of it are considered. Estimates of global features agree very well with state of the art guesses from other sources, and no strong dependence on the size of the window is appreciated at lowest levels. We find a Hubble constant of a bit more than 70 (km/s)/Mpc, a deceleration factor in the vicinity of -0.5 , and a current value of the dark energy parameter in the vicinity of -1 .

For further insight into the problem we have also performed reconstructions using a mock SNeIa sample depicting a future optimistic observational situation. The results support broadly what real data tell us, and in particular we find that dispersion in the data influences the reconstruction process a great deal.

And finally, using the binning method, we have obtained independent values of several quantities of interest. These may be useful for a quick/preliminary estimate of cosmological constraints without having to resort to a full dataset.

ACKNOWLEDGEMENTS

We are thankful to Diego Pavón for point out to us the interest of the works by Daly and Djorgovski. Irene Sendra holds a PhD FPI fellowship contract from the Spanish Ministry of Economy and Competitiveness. All three authors are supported by the mentioned ministry through research projects FIS2010-15492 and Consolider EPI CSD2010-00064, and also by the Basque Government through the special research action KATEA and the University of the Basque Country UPV/EHU under program UFI 11/55.

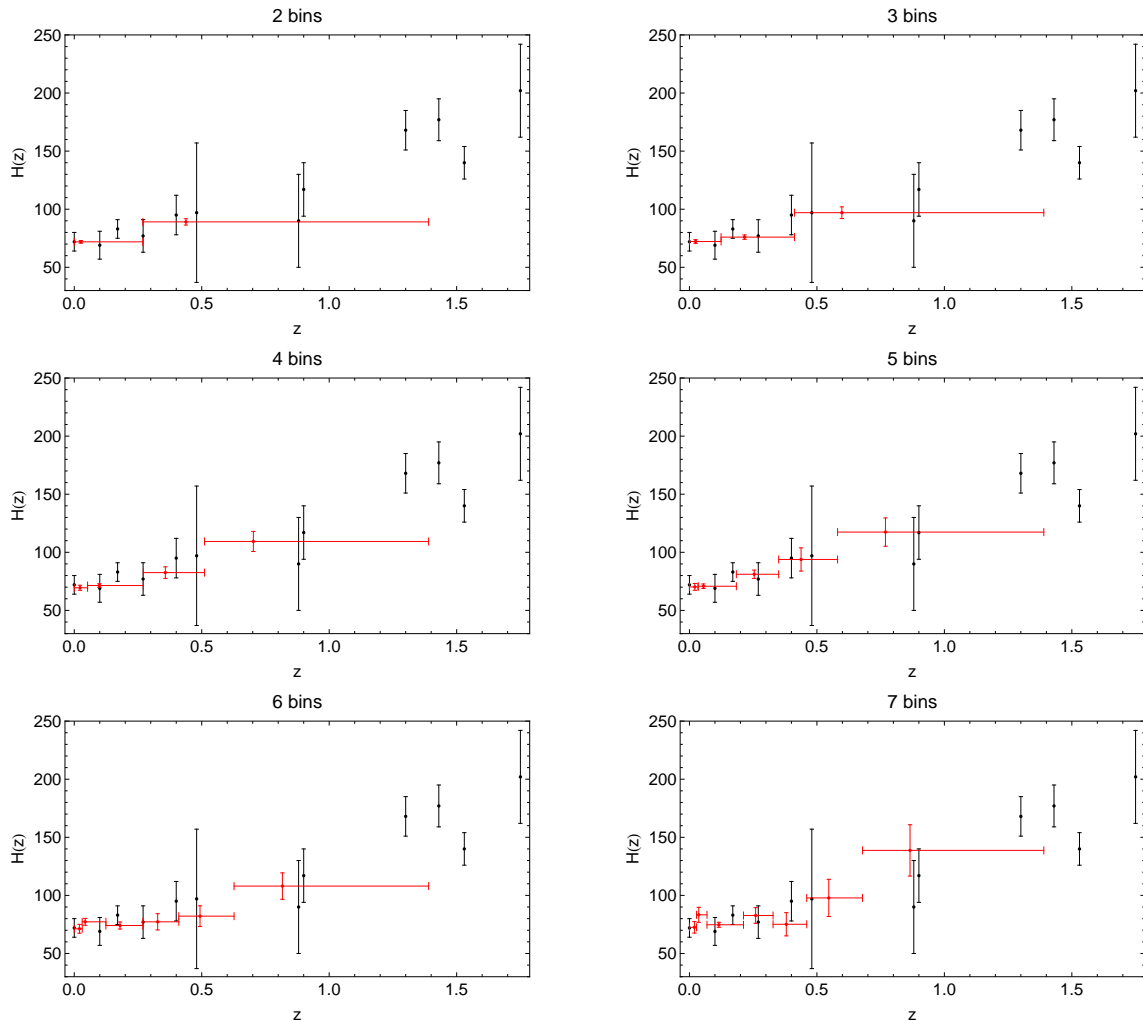


Figure 8. Values of $H(z)$ for the binned approach for different values of independent bins, red points. The central point indicates the median redshift of the bin with its corresponding error bars (vertical lines). The horizontal bars delimit the redshift bin. The $H(z)$ from [18] is also plotted (black points) in order to compare the results

-
- [1] A. G. Riess *et al.* [Supernova Search Team Collaboration], *Astron. J.* **116** (1998) 1009; S. Perlmutter *et al.* [Supernova Cosmology Project Collaboration], *Astrophys. J.* **517** (1999) 565-586.
- [2] D. Sapone, *Int. J. Mod. Phys. A* **25** (2010) 5253; J. Frieman, M. Turner, D. Huterer, *Ann. Rev. Astron. Astrophys.* **46** (2008) 385; V. Sahni, A. Starobinsky, *Int. J. Mod. Phys. D* **15** (2006) 2105.
- [3] D. Huterer, G. Starkman, *Phys. Rev. Lett.* **90** (2003) 031301; Y. Wang, M. Tegmark, *Phys. Rev. Lett.* **92** (2004) 241302; A. Shafieloo, U. Alam, V. Sahni, A. Starobinsky, *Mon. Not. R. Astron. Soc.* **366** (2006) 1081; U. Alam, V. Sahni, A. Starobinsky, *J. Cosmol. Astropart. Phys.* **06** (2004) 008; S. Nesseris, L. Perivolaropoulos, *Phys. Rev. D* **70** (2004) 043531; D. Huterer, A. Cooray, *Phys. Rev. D* **71** (2005) 023506; C. Shapiro, M.S. Turner, *ApJ* **649** (2006) 563; M.S. Turner, D. Huterer, *J. Phys. Soc. Japan* **11** (2007) 111015; U. Alam, V. Sahni, A. Starobinsky, *J. Cosmol. Astropart. Phys.* **11** (2007) 0702; V. Sahni, A. Starobinsky, *Int. J. Mod. Phys. D* **15** (2006) 2105; L. Perivolaropoulos, in *AIP Conf. Ser.* **848**, Recent Advances in Astronomy and Astrophysics (New York: AIP) 698 (2006).
- [4] R. A. Daly, S. G. Djorgovski, *Astrophys. J.* **597** (2003) 9.
- [5] R. A. Daly, S. G. Djorgovski, *Astrophys. J.* **612** (2004) 652.
- [6] R. A. Daly, S. G. Djorgovski, *Astrophys. J.* **677** (2008) 1.
- [7] A. C. Collazzi, B. E. Schaefer, A. Goldstein and R. D. Preece, arXiv:1112.4347 [astro-ph.HE], A. C. Collazzi, B. E. Schaefer and J. A. Moree, *Astrophys. J.* **729** (2011) 89.
- [8] A. Diaferio, L. Ostorero, V. F. Cardone, arXiv:1103.5501
- [9] http://lambda.gsfc.nasa.gov/product/map/dr4/params/wcdm_sz_lens_wmap7.cfm
- [10] R. Amanullah, *et al.*, *Astrophys. J.* **716** (2010) 712.

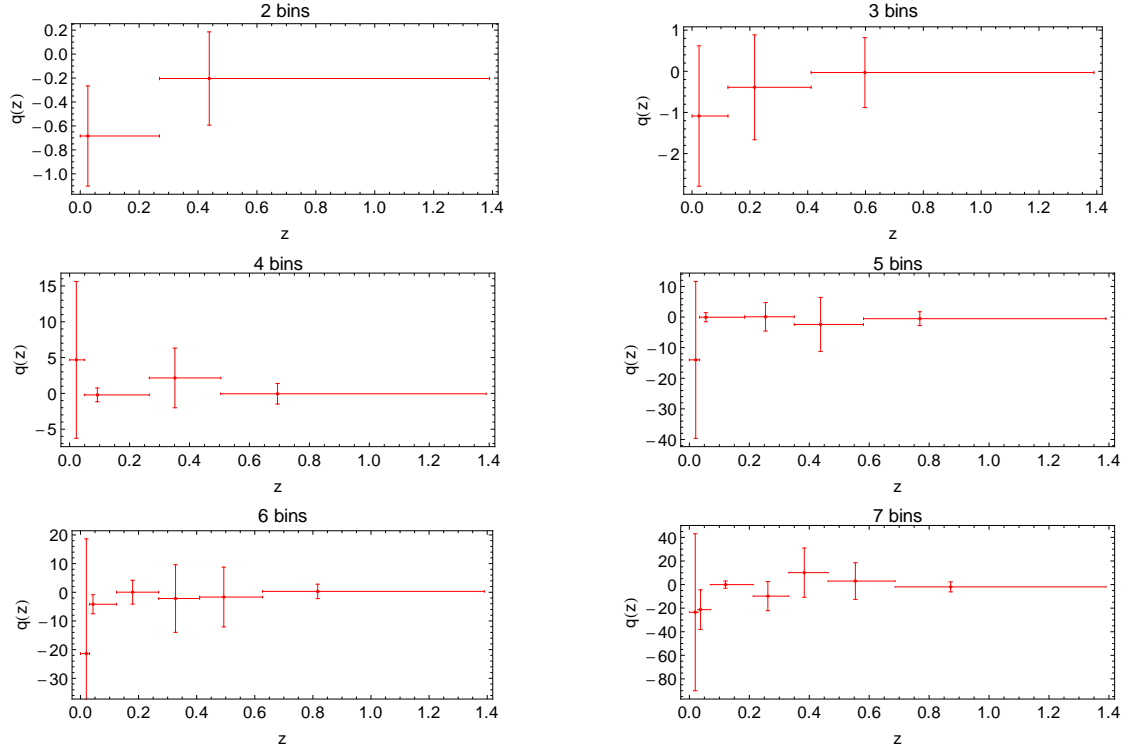


Figure 9. Values of $q(z)$ for the binned approach for different values of independent bins, red points. The central point indicates the median redshift of the bin with its corresponding error bars (vertical lines).

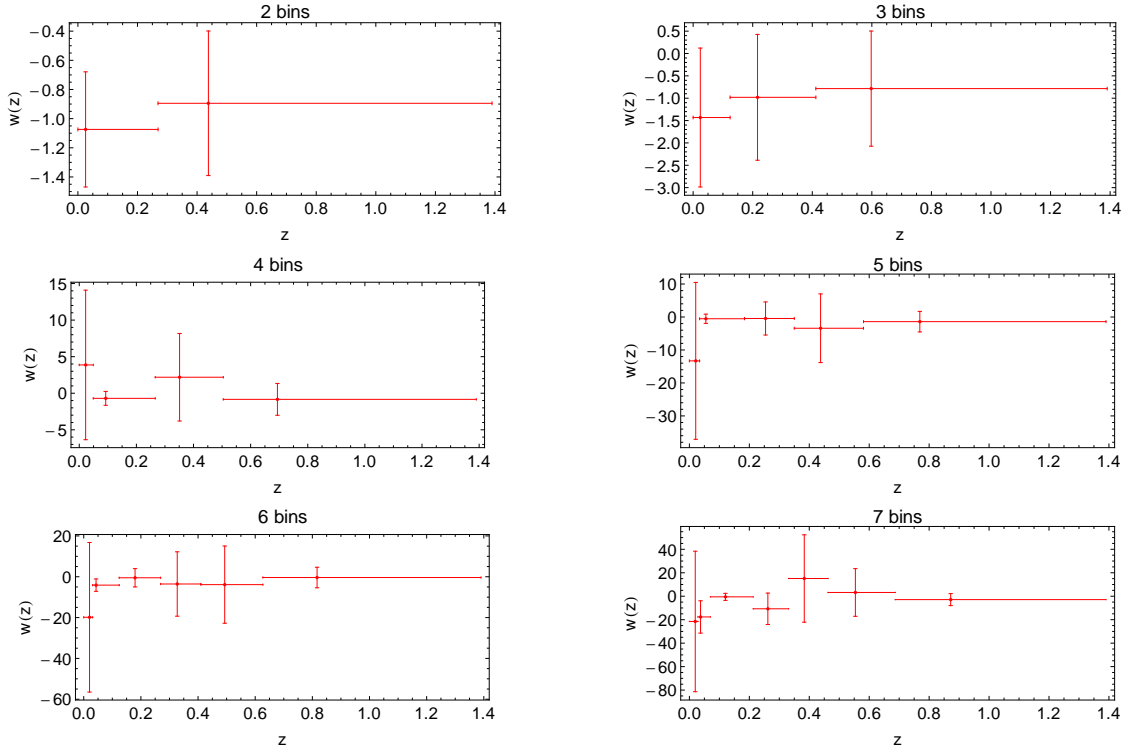


Figure 10. Values of $w(z)$ for the binned approach for different values of independent bins, red points. The central point indicates the median redshift of the bin with its corresponding error bars (vertical lines).

- [11] M. Kowalski, D. Rubin, G. Aldering, *et al.*, *Astrophys. J.* 686 (2008) 749.
- [12] R. Amanullah, *et al.*, *Astron. Astrophys.* 486 (2008) 375.
- [13] M. Hicken, *et al.*, *Astrophys. J.* 700 (2009) 331.
- [14] J. A. Holtzman, *et al.*, *Astron. J.* 136 (2009) 2306.
- [15] B. E. Schaefer, *Astrophys. J.* 660 (2007) 16.
- [16] A. G. Riess, L. Macri, S. Casertano, H. Lampeitl, H. C. Ferguson, A. V. Filippenko, S. W. Jha and W. Li *et al.*, *Astrophys. J.* **730** (2011) 119 [Erratum-ibid. **732** (2011) 129].
- [17] V. F. Cardone, S. Capozziello, M. G. Dainotti, *Month. Not. R. Astron. Soc.* 440 (2009) 775.
- [18] D. Stern, R. Jimenez, L. Verde, M. Kamionkowski, A. Stanford, *JCAP* 1002 (2010) 008.
- [19] Y. Wang, *Phys. Rev. D* 77 (2008) 123525.
- [20] A. Albrecht, (2006) [astro-ph/0609591](https://arxiv.org/abs/astro-ph/0609591).
- [21] M. Chevallier, D. Polarski, David, *Int. J. Mod. Phys. D* 10 (2001) 213.
- [22] E. V. Linder, *Phys. Rev. Lett.* 90 (2003) 091301.
- [23] C. Escamilla-Rivera, R. Lazkoz, V. Salzano and I. Sendra, *JCAP* **1109** (2011) 003.
- [24] J. Green, P. Schechter, C. Baltay, R. Bean, D. Bennett, R. Brown, C. Conselice and M. Donahue *et al.*, [arXiv:1108.1374](https://arxiv.org/abs/1108.1374) [[astro-ph.IM](https://arxiv.org/archive/astro)].
- [25] A. Albrecht, L. Amendola, G. Bernstein, D. Clowe, D. Eisenstein, L. Guzzo, C. Hirata, D. Huterer *et al.*, [[arXiv:0901.0721](https://arxiv.org/abs/0901.0721)]
- [26] G. Aldering, *et al.*, <http://snfactory.lbl.gov/snf/pdf/spie.2002.pdf>
- [27] A.G. Kim, E.V. Linder, R. Miquel, N. Mostek, *Month. Not. R. Astron. Soc.* 347 (2004) 909; A. Upadhye, M. Ishak, P. Steinhardt, *Phys. Rev. D* 72 (2005) 063501; M. Ishak, *Found. Phys.* 37 (2007) 1470.
- [28] I. Sendra, R. Lazkoz, [arXiv:1105.4943](https://arxiv.org/abs/1105.4943) [[astro-ph.CO](https://arxiv.org/archive/astro)] (*MNRAS* accepted).